THE JOURNAL OF BIOLOGICAL CHEMISTRY VOL. 285, NO. 50, pp. 39013–39020, December 10, 2010
Printed in the U.S.A.

Selective Electrodiffusion of Zinc Ions in a Zrt-, Irt-like Protein, ZIPB*◆

Received for publication, August 31, 2010, and in revised form, September 22, 2010 Published, JBC Papers in Press, September 28, 2010, DOI 10.1074/jbc.M110.180620

Wei Lin[‡], **Jin Chai**[‡], **James Love**[§], **and Dax Fu**[‡1]

From the [‡]*Biology Department, Brookhaven National Laboratory, Upton, New York 11973 and the* [§]*New York Structural Biology Center, New York City, New York 10027*

All living cells need zinc ions to support cell growth. Zrt-, Irt-like proteins (ZIPs) represent a major route for entry of zinc ions into cells, but how ZIPs promote zinc uptake has been unclear. Here we report the molecular characterization of ZIPB from *Bordetella bronchiseptica*, the first ZIP homolog to be purified and functionally reconstituted into proteoliposomes. Zinc flux through ZIPB was found to be nonsaturable and electrogenic, yielding membrane potentials as predicted by the Nernst equation. Conversely, membrane potentials drove zinc fluxes with a linear voltage-flux relationship. Direct measurements of metal uptake by inductively coupled plasma mass spectroscopy demonstrated that ZIPB is selective for two group 12 transition metal ions, Zn^{2+} and Cd^{2+}, whereas rejecting transition metal ions in groups 7 through 11. Our results provide the molecular basis for cellular zinc acquisition by a zinc-selective channel that exploits *in vivo* zinc concentration gradients to move zinc ions into the cytoplasm.

Zinc is an essential element for all living organisms (1). Zinc chemistry is widely exploited to drive enzymatic catalysis, organize protein structures, and mediate macromolecular interactions (2). In known proteomes, zinc-containing metalloproteins account for ~10% of the total proteins (3). Zinc metabolism is also very high. In human, ~1% of the total body zinc content is replenished daily by the diet (4). The abundant zinc utilization and its rapid turnover necessitate highly efficient zinc uptake mechanisms by which cells accumulate zinc to a total concentration in the submillimolar range (5). The vast majority of cellular zinc is in complex with specific protein partners (6). Free zinc ions, on the other hand, must be strictly limited in the cytoplasm to prevent cytotoxic side effects (7). Zinc efflux transporters and intracellular buffering systems are evolved to maintain an extremely low level of cytoplasmic free zinc, probably in a femtomolar to picomolar range (8, 9). When a zinc supply is available in the extracellular medium, the free zinc concentrations in the cytoplasm are expected to be many orders of magnitude lower than the extracellular zinc concentrations (10, 11). The inward zinc concentration gradients would provide a powerful chemical driving force to draw extracellular zinc ions into the cytoplasm if a transmembrane zinc conduit would connect the external zinc availability and the high intracellular zinc binding capacity. Such a zinc-specific uptake channel has not heretofore been identified.

A common assumption is that cellular zinc uptake is an active process mediated by metal transporters. In mammals, Zrt-, Irt-like protein (ZIP)[2] is the only zinc-specific uptake protein identified thus far (12). Although ZIPs supply zinc to meet cellular needs for growth, aberrant ZIP expressions have been linked to uncontrolled cell growth such as that occurring in cancer (13). Functionally, mammalian ZIPs promote zinc influx into the cytoplasm either from the extracellular medium or from zinc-enriched intracellular compartments (14). Members of the ZIP protein family are found at all phylogenetic levels (15). Plant, yeast, and bacterial ZIPs are relatively specific for zinc (16) as well as iron (17), and they are also implicated in transporting a broad spectrum of other transition metal ions, including Cd^{2+}, Co^{2+}, Cu^{2+}, and Mn^{2+} (18–20). To date, direct functional characterization of any ZIP homolog has been unattainable due to the technical bottleneck in overexpression and purification of ZIPs. Although none of ZIP homologs have been studied biochemically, they have been hypothesized to be ion-coupled secondary transporters (5). The assumed transport mechanism for ZIPs has largely been inferred from the observed saturable zinc uptake activities in cells expressing ZIP homologs (20–22). It is noted, however, that zinc influx and efflux are intricately linked in a zinc flow equilibrium around homeostatic set points (23). An elevated zinc influx may activate endogenous zinc efflux activities (24), resulting in a net zinc influx in a saturable manner. In light of this potential ambiguity, the mechanism of zinc uptake by ZIPs remains unclear.

In the present study, we obtained a heterologously expressed ZIP homolog from *Bordetella bronchiseptica*, termed ZIPB. The purified ZIPB was reconstituted into proteoliposomes, enabling detailed kinetic analysis of ZIPB-mediated metal fluxes under controlled experimental conditions. Our experiments demonstrate that ZIPB is a selective electrodiffusional channel. This result challenges the common assumption that cellular zinc uptake is an active process. Rather, ZIPB facilitates passive zinc uptake driven by zinc concentration gradients that are maintained by cellular zinc homeostasis.

* This work was supported, in whole or in part, by National Institutes of Health Grant R01 GM065137 (to D. F.) and by the Office of Basic Energy Sciences, United States Department of Energy, Grant DOE KC0304000 (to D. F.).

◆ This article was selected as a Paper of the Week.

[1] To whom correspondence should be addressed. Fax: 631-344-3407; E-mail: dax@bnl.gov.

[2] The abbreviations used are: ZIP, Zrt-, Irt-like proteins; DDM, *n*-dodecyl-β-D-maltopyranoside; TEA, tetraethylammonium; ICP-MS, inductively coupled plasma mass spectroscopy; CDF, cation diffusion facilitator; Ni-NTA, nickel-nitrilotriacetic acid; Bis-Tris, 2-(bis(2-hydroxyethyl)amino)-2-(hydroxymethyl)propane-1,3-diol.

EXPERIMENTAL PROCEDURES

Overexpression and Purification—ZIPB was selected through a high throughput screening process for expression and purification of membrane proteins (25, 26). For large scale overexpression, the ZIPB coding sequence was subcloned to pET15b with an N-terminal thrombin-cleavable hexa histidine tag. Overexpression of ZIPB was hosted in *Escherichia coli* C43(DE3) cells, grown in an auto-induction culture medium (27). Cells were harvested and mechanically ruptured using a Microfluidizer press cell. The membrane vesicles were solubilized in a detergent buffer containing 100 mM NaCl, 20 mM HEPES, pH 7.0, 7% *n*-dodecyl-β-D-maltopyranoside (DDM), 0.5 mM Tris(2-carboxyethyl) phosphine hydrochloride, 20% w/v glycerol, 1 mM $CdCl_2$, 10 mM K_2HPO_4/KH_2PO_4, and 10 mM imidazole. His-ZIPB was purified on an Ni-NTA superflow column. The His tag was removed by overnight thrombin digestion. The resulting ZIPB was concentrated to ~20 mg/ml and further purified by size-exclusion HPLC on a TSK 3000SW_{XL} column, pre-equilibrated with a mobile phase containing 20 mM NaOAc, pH 4.0, 100 mM NaCl, 12.5% glycerol, 0.03% DDM, 0.5 mM Tris(2-carboxyethyl) phosphine hydrochloride, 0.02 mM $ZnCl_2$. The molecular identity of the purified ZIPB was confirmed by mass spectrometric analysis on a Voyager-DE STR operated in matrix-assisted laser desorption/ionization time-of-flight (MALDI-TOF) linear mode.

Reconstitution and Stopped-flow Flux Measurements—Prior to reconstitution, HPLC-purified ZIPB, typically at ~20 mg/ml in the HPLC buffer, was diluted 20–400-fold with 1% *n*-octyl-β-D-glucoside to reduce the DDM concentration. The protocols for functional reconstitution, encapsulation of fluorescent indicators, stopped-flow measurements, and data analysis were described previously (28). Liposomes were made in parallel to proteoliposomes as a protein-free control. Stopped-flow experiments were carried out by mixing vesicles at a 1:1 ratio with an assay buffer at 8 °C. For measuring zinc fluxes in response to zinc concentration changes, the initial intravesicular $[Zn^{2+}]$ is zero, and extravesicular $[Zn^{2+}]$ increased from 0 to 2 mM in an assay buffer containing 50 mM K_2SO_4, 20 mM Bis-Tris-MES, pH 6.8. For measuring zinc fluxes in response to pH changes, the initial intravesicular $[Zn^{2+}]$ is zero, and extravesicular $[Zn^{2+}]$ was fixed at 0.5 mM. A broad pH range was buffered using 20 mM MES for pH from 5.0 to 7.0 and 20 mM Tris for pH from 7.0 to 9.0. At pH 7.0, zinc fluxes in the MES and Tris assay buffer were identical. For measuring zinc fluxes in response to membrane potential changes, 50 μM $ZnSO_4$ was added in equilibrium inside and outside of the vesicles. The vesicles were preloaded with either 50 mM K_2SO_4 or 50 mM $(TEA)_2SO_4$ and then exposed to an assay buffer containing a $K_2SO_4/(TEA)_2SO_4$ mixture with varied K^+-to-TEA^+ ratio at pH 6.8. Potassium ionophore valinomycin (2 μM) and voltage indicator oxonol VI (1 μM) were added to the vesicles and assay buffers, respectively. For measuring zinc fluxes in response to the proton motive forces, vesicles at a symmetrical $[Zn^{2+}]$ concentration of 50 μM were preloaded with either 50 mM K_2SO_4 or 50 mM $(TEA)_2SO_4$. The assay buffer contained either 50 mM K_2SO_4 or 50 mM $(TEA)_2SO_4$, respectively. An H^+/K^+ exchanger nigericin was added at 2 μM to the vesicles encapsulated with both FluoZin-1 and pyranine.

Metal Uptake Assay and ICP-MS Measurements—Metal uptake experiments were performed on 0.22-μm GS nitrocellulose filters. A metal ion as indicated was added to a final concentration of 0.2 mM to an assay buffer containing 20 mM Tris, 50 mM K_2SO_4, pH 7.0, with 2 mM $CaSO_4$ as the filter blocker. Proteoliposomes or liposomes were loaded onto filters mounted on a vacuum manifold and then overlaid with an ice-chilled, metal-containing assay buffer for 15 s at 8 °C. Next, the filters were washed with the metal-free assay buffer at an elevated pH of 9.0. The vesicles on the filter were then subject to acid digestion at 70 °C for 60 min using 60 μl of 70% nitric acid. The sample was clear of insoluble debris by a brief centrifugation, diluted with double distilled H_2O to a final HNO_3 concentration of 2%, and then analyzed on a PlasmaQuad 3 inductively coupled plasma mass spectrometer.

RESULTS

Homolog Screening—ZIP was nominated as a structural genomics target to the New York Consortium on Membrane Protein Structure (NYCOMPS). 52 bacterial and archaeal ZIP homologs were selected from a pool of 92 fully sequenced prokaryotic genomes based on a sequence similarity criterion (26). The chosen ZIP homologs were cloned, His-tagged, and overexpressed. An initial screen in a 96-well format identified 12 constructs that showed detectable protein expression by a His tag specific antibody. Scale-up expressions were followed, and proteins were partially purified by Ni-NTA affinity binding. Only 4 out of 12 constructs yielded expected protein bands on a Coomassie Blue-stained SDS-PAGE gel. This result is consistent with the general observation that ZIPs tend to be highly refractory to overexpression and purification. The level of ZIPB expression ranked third among the four positives, but ZIPB was the only homolog that remained soluble after a prolonged detergent incubation. Thus, ZIPB was singled out for large scale production.

Purification—ZIPB was heterologously overexpressed in *E. coli*, solubilized using DDM at a detergent-to-cell mass ratio of 1/10 (w/w), and then purified to homogeneity by Ni-NTA affinity chromatography (Fig. 1*a*). Western blot analysis showed that thrombin proteolysis completely removed the His tag (Fig. 1*a*). Initial size-exclusion high-performance liquid chromatography (HPLC) analysis, however, indicated that the majority of the purified ZIPB formed protein aggregates. Accordingly, a collection of detergents, metal ions, and buffers in various combinations was screened for an optimal stabilizing condition. The resulting ZIPB in a stabilized form was concentrated to ~20 mg/ml, and then subjected to preparative size-exclusion HPLC purification. The purified ZIPB showed a single monodispersed species with a retention time corresponding to an apparent molecular mass of 170 KDa in complex with detergents and lipids (Fig. 1*b*). MALDI-TOF mass spectrometric analysis of the peak fraction revealed a single mass species at 31,270 Da, in agreement with the expected molecular mass for ZIPB at 31,250 Da (Fig. 1*c*). The protein mass in the ZIPB-detergent-lipid complex was estimated to be ~62.9 kDa by size-exclusion HPLC coupled with in-line measurements of light

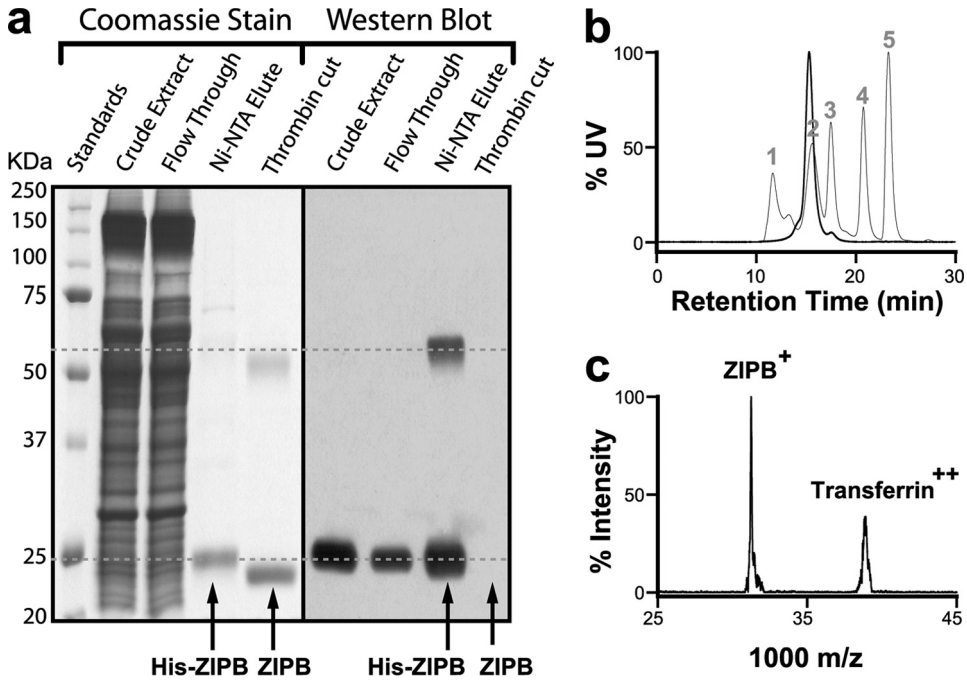

FIGURE 1. **Purification of ZIPB.** *a*, SDS-PAGE. Proteins as indicated in the purification process are revealed by Coomassie Blue stain (*left*) and Western blot using a His tag specific antibody (*right*). *Two dashed lines* mark the positions of the monomeric and dimeric His-ZIPB on the gel. *b*, analytical size-exclusion HPLC. *Thick line*, DDM-solubilized ZIPB. *Thin line*, protein standards: *1*, thyroglobulin (670 kDa); *2*, γ-globulin (158 kDa); *3*, ovalbumin (44 kDa); *4*, myoglobin (17 kDa); and *5*, vitamin B_{12} (1.35 kDa). *c*, MALDI-TOF mass spectrometry. The *m/z* reading was internally calibrated using transferrin. ZIPB, transferrin, and their charge states are labeled.

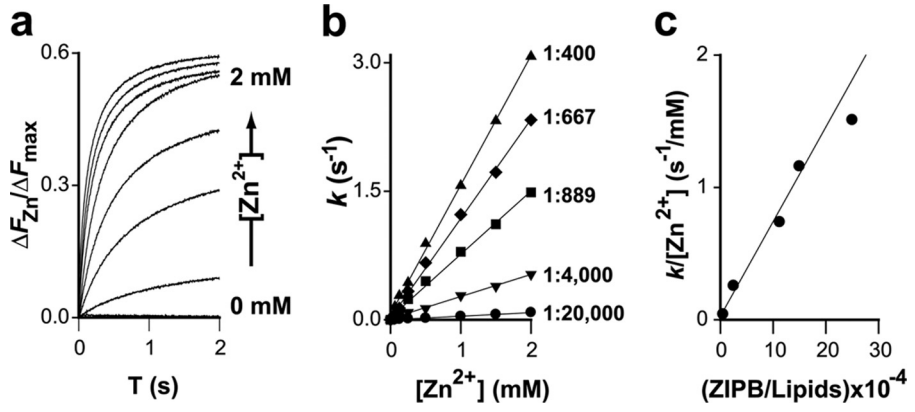

FIGURE 2. **ZIPB kinetics.** *a*, typical stopped-flow traces elicited by 1:1 mixing of proteoliposomes with an assay buffer containing $ZnSO_4$ to a final concentration from 0 to 2 mM as indicated. The *y* axis is the FluoZin-1 fluorescence change (ΔF_{Zn}) normalized to the maximum fluorescence change (ΔF_{max}). *b*, initial rate of zinc influx (*k*) as a function of the extravesicular zinc concentration. Each linear regression line was obtained from proteoliposomes with a fixed ZIPB/lipid molar ratio as indicated. *c*, the initial rate of zinc influx was normalized to the extravesicular zinc concentration. The resulting $k/[Zn^{2+}]$ was plotted as a function of the ZIPB/lipid molar ratio. The *solid line* represents a linear regression of the first four data points (ZIPB/lipid molar ratios range from 1:20,000 to 1:667). Note that the fifth data point at 1:400 deviates from the regression line as the proteoliposomes approach the maximum membrane-insertion capacity of ZIPB.

scattering, refractive index, and UV absorption (29). This protein mass is approximately equal to that of a ZIPB homodimer in the detergent micelles.

Functional Reconstitution—The HPLC-purified ZIPB was reconstituted into proteoliposomes by a detergent-mediated reconstitution method (28). The proteoliposomes were loaded with a fluorescent zinc indicator, FluoZin-1, and then exposed to various zinc-containing assay buffers. Zinc fluxes in response to rapid zinc exposures were detected by stopped-flow fluorometry. The net zinc influx (ΔF_{Zn}) through the reconstituted ZIPB was obtained by subtracting the background zinc leakage measured from control liposomes. The background leakage was negligible when compared with the ZIPB-mediated flux. The total vesicle loading of FluoZin-1 was quantified as the maximum fluorescence change (ΔF_{max}) in response to detergent dissolution of vesicles that released all the encapsulated FluoZin-1 to 2 mM extravesicular Zn^{2+} (28). Normalizing ΔF_{Zn} to ΔF_{max} resulted in a dimensionless fluorescence change, $\Delta F_{Zn}/\Delta F_{max}$. Fig. 2*a* shows typical recordings of $\Delta F_{Zn}/\Delta F_{max}$ that rose exponentially upon rapid exposures of proteoliposomes to extravesicular zinc with increasing concentrations from 0 to 2 mM.

Concentration Dependence—Zn^{2+} influxes were measured at a fixed ZIPB-to-lipid molar ratio with varied extravesicular zinc concentrations or at a fixed extravesicular zinc concentration with varied ZIPB-to-lipid ratios. The initial rate of the fluorescence response was found to be directly proportional to the zinc concentration with no evidence of saturation up to an extravesicular zinc concentration of 2 mM (Fig. 2*b*). A control experiment was performed using a well characterized zinc efflux transporter, YiiP (30, 31). Under the same experimental conditions, YiiP exhibited the typical saturation kinetics expected for a carrier-mediated flux. Thus, the zinc flux through ZIPB was indeed nonsaturating within the physiological zinc concentration range. The rate of zinc flux normalized to the extravesicular zinc concentration also increased linearly with the ZIPB-to-lipid molar ratio within a range from 1:20,000 to 1:667 (Fig. 2*c*). At a higher ratio of 1:400, the normalized zinc flux rate seemed to fall off the regression line (Fig. 2*c*). Thus, the upper bound protein-to-lipid molar ratio for ZIPB reconstitution is between 1:667 and 1:400. This value suggested that the reconstitution of ZIPB is slightly more efficient than the membrane insertion of ATP binding cassette transporters under optimized reconstitution conditions (32).

Electrodiffusion—The observed first order kinetics suggested that the ZIPB-mediated zinc flux may represent passive electrodiffusion. If this is the case, a zinc flux down its concentration gradient would generate a transmembrane potential according

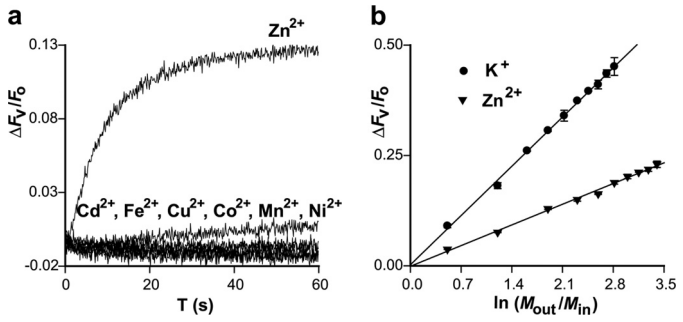

FIGURE 3. **Electrogenic effect.** *a*, voltage change ($\Delta F_v/F_o$) in response to imposition of an inward metal concentration gradient (1 mM outside and 0 mM inside). A metal ion as indicated was mixed with proteoliposomes, and the corresponding oxonol VI fluorescence change (ΔF_v) relative to its baseline reading (F_o) was plotted as a function of time. *b*, Nernst relationship between the quasi-stationary oxonol VI signal ($\Delta F_v/F_o$) and the gradient of zinc (*filled triangle*) or potassium (*filled circle*) expressed in logarithm of the extravesicular-to-intravesicular concentration ratio (M_{out}/M_{in}). Linear regressions (*solid line*) yielded a slope of 0.16 ± 0.01 for Zn^{2+} and 0.36 ± 0.01 for K^+, respectively. Data are presented as means ± S.E. of a triplicate experiment.

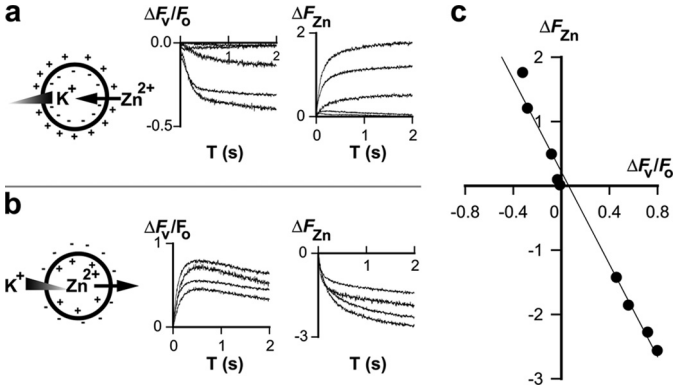

FIGURE 4. **Membrane potentials drive bidirectional zinc fluxes.** *a*, an outward potassium gradient trigged an inside-negative membrane potential and an inward zinc flux as illustrated (*left*). The membrane potential change ($\Delta F_v/F_o$) was monitored by the oxonol VI fluorescence as a function of time (*middle*), whereas the zinc influx (ΔF_{Zn}) was indicated by the FluoZin-1 fluorescence change as a function of time (*right*). *b*, an inward potassium gradient trigged an inside-positive membrane potential and an outward zinc flux. *c*, flux-voltage relationship. The *x* and *y* axis are respectively the quasi-stationary $\Delta F_v/F_o$ and ΔF_{Zn} response taken from *a* and *b*. The *solid line* represents a linear regression that relates the zinc flux to the membrane potential.

to the Nernst equilibrium. The membrane potential was detected using a fluorescent potentiometric indicator, oxonol VI, that can respond to the membrane potential linearly under our experimental conditions (33). An exposure of proteoliposomes to 1 mM extravesicular Zn^{2+} rapidly developed an inside-positive potential, as indicated by a rise of oxonol VI fluorescence (Fig. 3*a*). The electrogenic effect was attributed to the zinc influx because proteoliposomes preloaded with 1 mM Zn^{2+} in equilibrium with the extravesicular zinc concentration did not yield detectable change in oxonol VI fluorescence. The electrogenic effect seemed specific to zinc. Among a set of divalent metal ions examined, Zn^{2+} was the only metal ion that elicited a significant voltage response (Fig. 3*a*).

Within an extravesicular zinc concentration ranging from 0.25 to 4.5 mM, zinc influxes rapidly filled up the proteoliposomes to the maximum filling capacity, corresponding to an intravesicular zinc concentration of 0.15 mM, as estimated according to the quasi-stationary $\Delta F_{Zn}/\Delta F_{max}$ readings (Fig. 2*a*). Apparently, zinc influxes built up membrane potentials in opposition to chemical driving forces of the zinc concentration gradients. Accordingly, the oxonol VI response was found to be linear to the zinc driving force, $(RT/FZ)\ln[(Zn^{2+})_{out}/(Zn^{2+})_{in}]$, where *R*, *T*, and *F* are thermodynamic constants, and *Z* is the ionic valence of the permeant ion (Fig. 3*b*). An internal calibration of the oxonol VI response was performed using a series of potassium concentration gradients down a potassium ionophore valinomycin (34). Increasing $[K^+]_{out}$ from 0.5 mM to 5 mM yielded a linear increase of the quasi-stationary oxonol VI response (Fig. 3*b*). Under the identical experimental conditions, except that the monovalent K^+ was in place of the divalent Zn^{2+}, a $[K^+]_{in}$ of 0.3 mM was expected to reach the proteoliposome filling capacity. The slope of the K^+ regression line approximately doubled that of the Zn^{2+} regression line (Fig. 3*b*), as predicted by a 2-fold valence difference of the Nernst equation. These observations draw a parallel between ZIPB and a potassium ionophore that functions as an ion-selective electrodiffusional pore.

Further supporting evidence for electrodiffusional fluxes through ZIPB came from simultaneous measurements of zinc fluxes and membrane potentials using FluoZin-1 and oxonol VI, respectively. Proteoliposomes were loaded with 50 μM Zn^{2+} in equilibrium with the extravesicular Zn^{2+} concentration. At this symmetrical zinc concentration, zinc fluxes were driven by imposition of transmembrane potentials, which were generated by applying K^+ transmembrane gradients across valinomycin. Bidirectional K^+ concentration gradients were elicited by rapidly exposing proteoliposomes to an assay buffer with varied K^+-to-TEA^+ concentration ratios. As shown in Fig. 4*a*, outward K^+ gradients induced negative oxonol VI responses accompanied by increases of the FluoZin-1 fluorescence. The concurrent fluorescence changes indicated that an inside-negative membrane potential induced a zinc influx. Conversely, inward K^+ gradients triggered inside-positive membrane potentials, which drove zinc effluxes (Fig. 4*b*). A correlation between the quasi-stationary FluoZin-1 and oxonol VI responses showed a linear relationship between the zinc fluxes and the membrane potentials (Fig. 4*c*). This ohmic behavior at a symmetrical zinc concentration obeys the Goldman-Hodgkin-Katz current equation with an underlying mechanism ascribed to passive electrodiffusion (35). Characterization of voltage dependence of zinc flux under an asymmetrical condition was limited by a small FluoZin-1 detection window set by a lower bound detection limit of FluoZin-1 and an upper bound limit of its linear range (28).

Temperature Dependence—Zinc fluxes through ZIPB were measured at six different temperatures from 3 to 18 °C (Fig. 5). The initial rate of zinc flux induced by 0.5 mM extravesicular zinc showed a weak temperature dependence, corresponding to an activation energy of 8.2 ± 0.8 kJ/mol. This value is significantly lower than the typical range of activation energies for membrane transporters, *e.g.* 50–60 kJ/mol for a Na/Ca exchanger (36) or 81 kJ/mol for transport of Cs^+ through an organic cation transporter rOCT2 (37). The temperature-dependent data of ZIPB are compatible with an electrodiffusional process that requires minimal conformational changes.

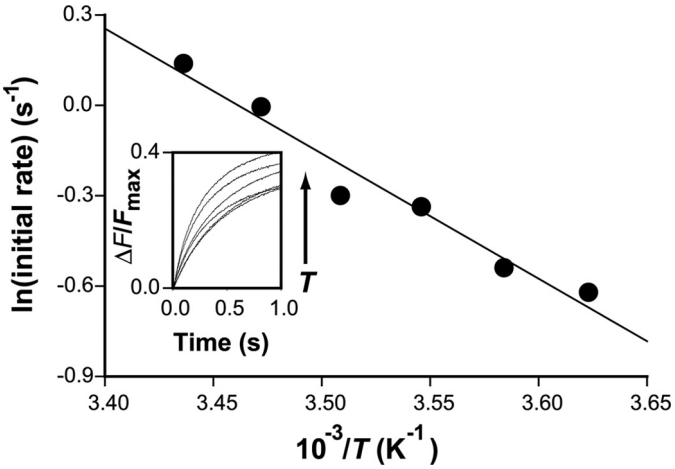

FIGURE 5. **Arrhenius plot of zinc fluxes at 3, 6, 9, 12, 15, and 18 °C.** *x* axis, the reciprocal of temperature; *y* axis, the initial rate of zinc flux on a logarithmical scale. The *solid line* represents a linear regression of the temperature dependence. *Inset*, FluoZin-1 traces ($\Delta F_{Zn}/F_{max}$) recorded as a function of time at various temperatures.

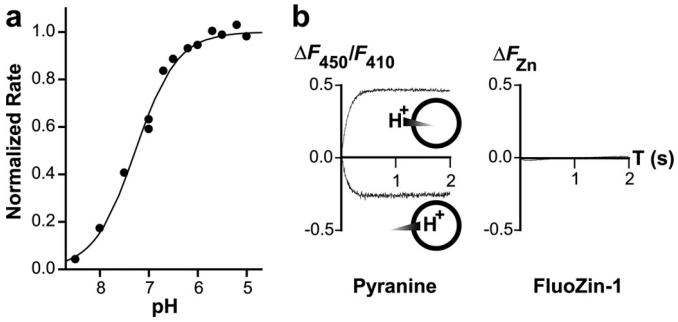

FIGURE 6. **pH dependence.** *a*, the initial rate of zinc flux was normalized to the flux rate at pH 5 and then plotted as a function of the pH ranging from 5 to 9. The pH dependence was fitted to the Hill equation (*solid line*) with fitting parameters given under "Results." *b*, zinc flux is not coupled to the proton motive force. Bidirectional transmembrane proton gradients were monitored by the fluorescence difference ($\Delta F_{450}/F_{410}$) of pyranine (*left*), but no zinc flux in either direction was detected by FluoZin-1 (*right*). Note that an increase or decrease of the pyranine fluorescence indicates an increase or decrease of intravesicular pH, respectively.

pH Dependence—H^+ and K^+ are the only two physiological ion species besides Zn^{2+} in the assay buffer. Zinc flux remained unchanged by a complete substitution of K^+ with TEA^+, but was reduced to the background level by alkalinization of the assay buffer to pH 9.0. The pH dependence of ZIPB was examined using aliquots of proteoliposomes, pre-equilibrated at a pH ranging from 5 to 9. The initial rate of Zn^{2+} influx in response to 0.5 mM extravesicular Zn^{2+} increased progressively with the H^+ concentration (Fig. 6*a*). The observed $[H^+]$ dependence was fit to the Hill equation, yielding a $K_{0.5} = 53.1 \pm 3.8$ nM and a stoichiometry $n = 1.0 \pm 0.1$. A near unity n value suggested a noncooperative proton effect. At pH 6.8 and at a symmetrical Zn^{2+} concentration of 50 μM, a transmembrane H^+ gradient was applied to proteoliposomes using an electroneutral H^+/K^+ exchanger, nigericin, that can convert an imposed K^+ gradient to a proton gradient (38). Changes in intravesicular $[Zn^{2+}]$ and $[H^+]$ were monitored simultaneously by dual encapsulation of FluoZin-1 and a pH indicator, pyranine (39). An inward K^+ gradient, corresponding to inside 0 mM K^+ + 100 mM TEA^+ and outside 50 mM K^+ + 50 mM TEA^+, caused an increase in pyranine fluorescence, whereas an outward K^+ gradient, corresponding to inside 100 mM K^+ + 0 mM TEA^+ and outside 50 mM K^+ + 50 mM TEA^+, elicited a pyranine response in the opposite direction (Fig. 6*b*). No zinc flux was detected in response to the proton gradient in either direction. In contrast, under the identical experimental conditions, robust bidirectional Cd^{2+} fluxes were reported through a proton-coupled zinc efflux transporter, ZitB (28). Taken together, ZIPB-mediated zinc flux is dependent upon pH, but independent of the proton motive force.

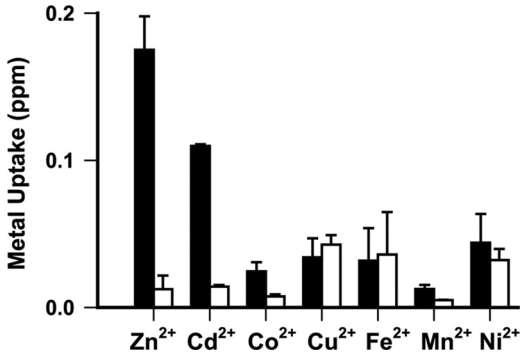

FIGURE 7. **Metal selectivity.** Total metals (metals trapped inside the vesicles plus metals bound to the filter) were quantified in ppm by ICP-MS. Background metal levels on the filter were estimated using an equivalent filter without deposited vesicles. Subtracting the background metal levels from the total metal readings yielded the net metal uptake for proteoliposomes (*closed bar*, $n = 4$) and liposomes (*open bars*, $n = 4$). Data are presented as means ± S.E.

Metal Selectivity—Metal selectivity was directly assessed using ICP-MS. This mass spectrometric approach allows quantitative multi-element analysis. The metal uptake reaction was performed on a membrane filter on which the proteoliposomes were washed free of extravesicular metal ion by a high pH assay buffer that minimized metal backflow through ZIPB. A 15-s exposure of the protein-free liposomes to metal ions at an extravesicular concentration of 0.2 mM yielded only background level signals, whereas ZIPB proteoliposomes under the same experimental condition accumulated Zn^{2+} 12-fold above the background (Fig. 7). Of the six additional metal ions examined, Cd^{2+} was the only one that showed significant accumulation into proteoliposomes, although the rate of Cd^{2+} accumulation seemed slower than that of Zn^{2+}. The ZIPB-mediated Cd^{2+} influx was confirmed by stopped-flow FluoZin-1 fluorescence measurements. Moreover, Zn^{2+} and Cd^{2+} uptakes were mutually inhibited by each other but not by any other metal ions examined. This observation suggested a competition between Zn^{2+} and Cd^{2+} for ZIPB. It was noted that the Cd^{2+} influx did not yield an oxonol VI fluorescence change (Fig. 3*a*). Intriguingly, a membrane potential induced by an inward potassium concentration gradient across valinomycin was found to drive Cd^{2+} efflux through ZIPB at a symmetrical Cd^{2+} concentration. The mechanism underpinning the difference between the electrogenic effects of Zn^{2+} and Cd^{2+} influx is unclear.

DISCUSSION

The experiments described herein demonstrate that the purified ZIPB protein alone can mediate a transmembrane zinc

```
ZIPB              MNQPSSLAADLRGAWHAQAQSHPLITLGLAASAAGVVLLLVAGIVNALTGENRVHVGYAVLGGAAGFAATALGALMALGL  60
ZupT, E. coli     ------------------------------------------------------MSVPLILTILAGAATFIGAFLGVLG  25
ZIP, Arabidopsis  -----------------------------------------------------MDSQMLVALGLSLVGGLSTSLGALFVVLS  29
ZIP11, Human      ----------------------------------------------MLQGHSSVFQALLGTFFTWGMTAAGAALVFVF  32

ZIPB              RAISARTQDAMLGFAAGMMLAASAFSLILPGLDAAGTIVGPGPAAAAVVALGLGLGVLLMLGLDYFTPHEHERTGHQGPE 160
ZupT, E. coli     QKPSNRLLAFSLGFAAGIMLLISLMEMLPAALAAEG---------MSPV---LGYGMFIFGLLGYFGLDR-MLPHAHPQD 92
ZIP, Arabidopsis  ETPNMKMLGLLQGFASGLMLSISFLDLAHNAINSIG---------FFKANLWFFGGVIFFACITKFIPEP-TLGPSTDGK 99
ZIP11, Human      SSGQRRILDGSLGFAAGVMLAASYWSLLAPAVEMATSSGGFGAFAFFPVAVGFTLGAAFVYLADLLMPHL.ALALNFGST 119

                                  Putative TM4
ZIPB              AARVNRVWLFVLTIILHNLPEGMAIGVSFATGDLRIGLPLTSAIAIQDVPEGLAVALALRAVGLPIGRAVLVAVASGLME 240
ZupT, E. coli     LMQKS..ILLTLGISLHNFPEGIATFV-TASSNLELGFGIALAVALHNIPEGLAVAGPVYAATGSKRTAILWAGISGLAE 181
ZIP, Arabidopsis  RRKKN..LITAIGISLHNFPEGMAVFL-GSIKGMRVGVNLALAIALHNIPEGVAVALPIYFATESKWQAFKLATLSGLAE 196
ZIP11, Human      LMKK.RIALLILAITIHNVPEGLAVGV.TASATFESARNLAIGIGIQNFPEGLAVSLPLRGAGFSTWRAFWYGQLSGMVE 266

ZIPB              PLGALVGVGISSGFALAYPISMGLAAGAMIFVVSHEVIPETHRNGHETTATVGLMAGFALMMFLDTALG--------- 309
ZupT, E. coli     ILGGVL.ILGSMISPVVMAAIMAVVAGIMVALSVDELMPLAKEIDPNNNPSYGVLCGMSVMGFSLVLLQTAGIG---- 257
ZIP, Arabidopsis  PLGVII.LFPRSLSPEILEGLLGAVGGIMAFLTLHEMLPLAFDYAGQKQAVKAVFFGMACMSASLYFLELSLPETMSL 276
ZIP11, Human      PLAGVFGAFAVVLAEPILPYALAFAAGAMVYVVMDDIIPEAQISGNGKLASWASILGFVVMMSLDVGLG--------- 335
```

FIGURE 8. **Sequence alignment.** ZIPB (NP_888945) was aligned with ZIP homologs from *E. coli* (YP_002409442), *Arabidopsis thaliana* (NP_566669), and human (NP_631916). Identical and highly conserved residues are colored in *red* and *brown*, respectively. *Dots* indicate omitted resides, and *dashed lines* represent residue gaps in the alignment. The *blue box* marks the ZIP signature sequence in the putative TM4 as highlighted.

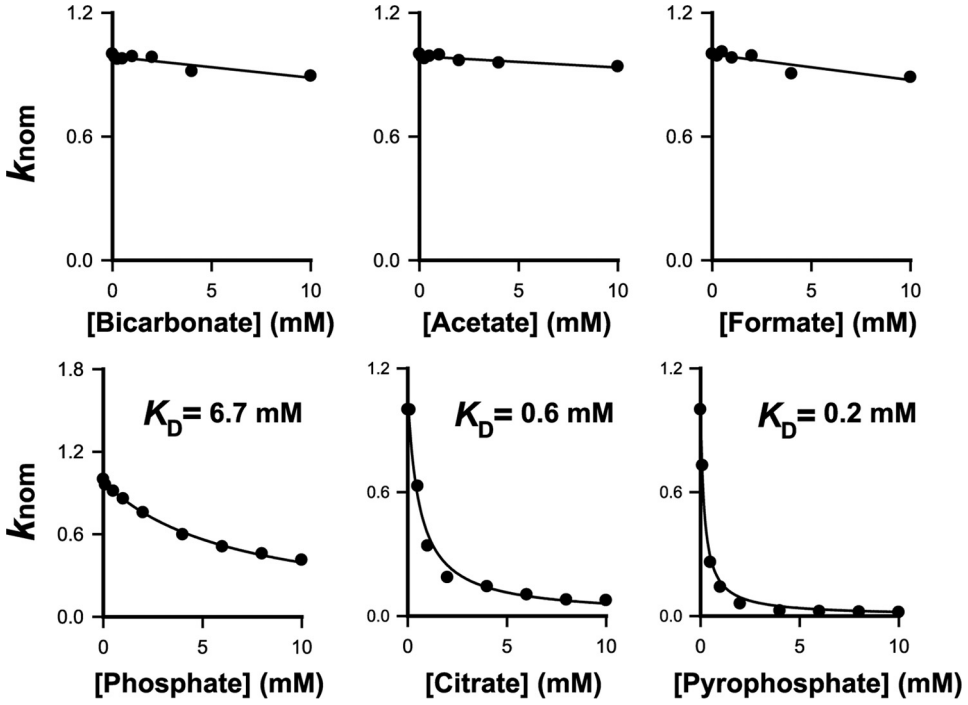

FIGURE 9. **The effects of anions on zinc flux through ZIPB.** The initial rate of zinc flux in response to 0.5 mM extravesicular zinc ion was measured in the presence of an indicated anion that was added to the assay buffer at a concentration ranging from 0 to 10 mM. k_{nom} is a dimensionless rate constant obtained by normalizing the zinc flux rate to the maximum rate at 0 mM anion. Assuming Zn^{2+} and the anion A form a binary complex with an apparent dissociation constant K_D, the values of K_D were obtained by least squares fitting (*solid line*) of the anion concentration dependence to a hyperbolic equation, $k_{nom} = K_D/(K_D+[A])$.

flux that is nonsaturable, electrogenic, and voltage-dependent. The zinc equilibrium potential exhibits a Nernst relationship predicted for divalent Zn^{2+} with reference to monovalent K^+. The voltage dependence of the zinc flux also follows the Goldman-Hodgkin-Katz current equation at a symmetrical zinc concentration. These data provide strong evidence that the ZIPB-mediated zinc flux truly represents electrodiffusion through a zinc-permeant channel. All ZIPs identified thus far promote zinc influx into the cytoplasm where zinc is buffered to extremely low levels around homeostatic set points (40). From an energetic standpoint, ZIPB may provide a zinc conduit in the membrane barrier that allows zinc to flow into cells down the concentration gradient maintained by cellular zinc homeostasis. The presence of an inside-negative membrane potential would further aid zinc electrodiffusion. Given the zinc homeostatic concentration gradients in living cells, the electrodiffusion ascribed to ZIPB may represent a general mechanism by which cells acquire zinc to satisfy their metabolic needs for growth.

Most ZIPs are eight-spanner membrane proteins and share a transmembrane topology with both N termini and C termini located on the extracytoplasmic side of the membrane. Highly conserved sequences clustered around the putative transmembrane segment 4 define a signature sequence for the ZIP family (15). The signature sequence is well preserved in ZIPB (Fig. 8), indicating that ZIPB is a *bona fide* member of the ZIP family. ZIPB is a structural genomic target selected from a large collection of microbial ZIP homologs. Despite its prokaryotic origin, ZIPB also shows a significant homology to some eukaryotic counterparts, *e.g.* a 38% sequence identity with human ZIP11 for 160 residues in the C-terminal half of the proteins (Fig. 8). This observation agrees with the notion that the C-terminal half of ZIP homologs is better conserved than the N-terminal half (15).

Until now, the selectivity of ZIPs has been inferred from indirect analyses of genetic complementation and mutant phenotypes (16–20). Our ICP-MS data provide direct evidence that ZIPB is permeable to Zn^{2+} and Cd^{2+} but not Fe^{2+}, Cu^{2+}, Co^{2+}, Mn^{2+}, and Ni^{2+}. ZIPB shares a common metal selectivity with YiiP, a metal efflux transporter in the cation diffusion facilitator (CDF) family (41). The purified YiiP is selective for Zn^{2+} and Cd^{2+} against Fe^{2+}, Cu^{2+}, Co^{2+}, Mn^{2+}, and Ni^{2+} (30), although YiiP exhibited a ferrous tolerance phenotype in a mutant *E. coli* strain (42). Both zinc and cadmium are group 12 transition metals. They prefer tetrahedral coordination, whereas all rejected metals favor higher coordination numbers, belonging to groups 7 through 11 of the periodic table. It seems plausible that ZIPB discriminates among various metal ions based on their coordination chemistries. This coordination-based selective mechanism is supported by the crystal structure of YiiP, which revealed a zinc-occupied tetrahedral coordination site in the zinc translocation pathway (43). A shared metal selectivity between YiiP and ZIPB suggests a recurring structural theme in which a zinc ion may obligatorily bind to a tetrahedral coordination site in ZIPB during its passage through the membrane.

Cellular zinc homeostasis critically depends on the flux equilibrium between zinc uptake through ZIPs and zinc efflux through CDFs (44). At present, overexpression of eukaryotic zinc transporters remains technically challenging. The bacterial YiiP and ZIPB serve as prototypes for CDFs and ZIPs, respectively. CDFs utilize the proton motive force to actively pump zinc out of the cytoplasm (28, 45), whereas ZIPs operate passively in an opposite direction (5). The uphill pumping of zinc in YiiP is driven by a downhill flow of protons, whereas zinc passage in ZIPB is independent of the proton motive force. Previous work suggested that bicarbonate may stimulate the zinc uptake activity of hZIP2 in K562 erythroleukemia cells (20). Our data showed, however, that ZIPB is fully active in the absence of any physiological ion except for proton. Zinc flux measurements also showed no evidence of stimulatory effects on ZIPB by bicarbonate and other common organic anions (Fig. 9). Rather, phosphate, citrate, and pyrophosphate significantly reduced the zinc flux rate in a concentration-dependent manner. The rank order of apparent dissociation constants for phosphate, citrate, and pyrophosphate is consistent with the expected rank order for their stability constants for zinc. Our data thus suggest that the observed inhibitory effects are likely attributed to metal chelation effects.

The ZIPB-mediated zinc flux is nonsaturating with respect to a zinc concentration up to 2 mM. Nevertheless, the zinc flux through ZIPB is extremely slow in comparison with the potassium ion flux in potassium channels. The marked difference in ion flux rates may reflect the physiological role that ZIPB plays in zinc homeostasis as opposed to transient cell signaling. Interestingly, a direct comparison of zinc flux rates for ZIPB and YiiP at 2 mM extravesicular zinc showed that ZIPB was considerably slower than YiiP in transporting zinc ions at physiological conditions. The slower zinc flow in ZIPB likely allows the putative zinc coordination site to operate under its saturation limit, thus giving rise to nonsaturating kinetics. The restricted zinc flow further implies channel constriction(s) that may exist along the zinc conduit. At present, structures of ZIPB and any other ZIP homologs are unknown. The purification of ZIPB in a functional form lays the groundwork for structural analysis of an archetypal ZIP homolog.

Acknowledgments—We thank Bill Studier for comments, Marco Punta for bioinformatics support, Renato Bruni for cloning and expression of ZIPB homologs, and Babak Andi for proofreading of the manuscript. NYCOMPS is supported by the National Institutes of Health (Grant 5U54GM075026 to W. Hendrickson). Brookhaven National Laboratory (BNL) is managed by Brookhaven Science Associates for the United States Department of Energy.

REFERENCES

1. Vallee, B. L., and Auld, D. S. (1990) *Biochemistry* **29,** 5647–5659
2. Vallee, B. L., and Falchuk, K. H. (1993) *Physiol. Rev.* **73,** 79–118
3. Dupont, C. L., Yang, S., Palenik, B., and Bourne, P. E. (2006) *Proc. Natl. Acad. Sci. U.S.A.* **103,** 17822–17827
4. King, J. C., and Cousins, R. J. (2005) *in Modern Nutrition in Health and Disease* (Shils, M. E., Shike, M., Ross, A. C., Caballero, B., and Cousins, R. J., eds) pp. 271–285, Lippincott Williams & Wilkins, Baltimore, MD
5. Eide, D. J. (2006) *Biochim. Biophys. Acta* **1763,** 711–722
6. Krezel, A., and Maret, W. (2006) *J. Biol. Inorg. Chem.* **11,** 1049–1062
7. Koh, J. Y., Suh, S. W., Gwag, B. J., He, Y. Y., Hsu, C. Y., and Choi, D. W. (1996) *Science* **272,** 1013–1016
8. Outten, C. E., and O'Halloran, T. V. (2001) *Science* **292,** 2488–2492
9. Bozym, R. A., Thompson, R. B., Stoddard, A. K., and Fierke, C. A. (2006) *ACS Chem. Biol.* **1,** 103–111
10. Magneson, G. R., Puvathingal, J. M., and Ray, W. J., Jr. (1987) *J. Biol. Chem.* **262,** 11140–11148
11. Sensi, S. L., Paoletti, P., Bush, A. I., and Sekler, I. (2009) *Nat. Rev. Neurosci.* **10,** 780–791
12. Cousins, R. J., Liuzzi, J. P., and Lichten, L. A. (2006) *J. Biol. Chem.* **281,** 24085–24089
13. Taylor, K. M., Morgan, H. E., Smart, K., Zahari, N. M., Pumford, S., Ellis, I. O., Robertson, J. F., and Nicholson, R. I. (2007) *Mol. Med.* **13,** 396–406
14. Eide, D. J. (2004) *Pflugers Arch.* **447,** 796–800
15. Eng, B. H., Guerinot, M. L., Eide, D., and Saier, M. H., Jr. (1998) *J. Membr. Biol.* **166,** 1–7
16. Zhao, H., and Eide, D. (1996) *Proc. Natl. Acad. Sci. U.S.A.* **93,** 2454–2458
17. Eide, D., Broderius, M., Fett, J., and Guerinot, M. L. (1996) *Proc. Natl. Acad. Sci. U.S.A.* **93,** 5624–5628
18. Korshunova, Y. O., Eide, D., Clark, W. G., Guerinot, M. L., and Pakrasi, H. B. (1999) *Plant Mol. Biol.* **40,** 37–44
19. Grass, G., Franke, S., Taudte, N., Nies, D. H., Kucharski, L. M., Maguire, M. E., and Rensing, C. (2005) *J. Bacteriol.* **187,** 1604–1611
20. Gaither, L. A., and Eide, D. J. (2000) *J. Biol. Chem.* **275,** 5560–5564
21. Dufner-Beattie, J., Langmade, S. J., Wang, F., Eide, D., and Andrews, G. K. (2003) *J. Biol. Chem.* **278,** 50142–50150
22. Gaither, L. A., and Eide, D. J. (2001) *J. Biol. Chem.* **276,** 22258–22264
23. Nies, D. H. (2007) *Science* **317,** 1695–1696
24. Lu, M., Chai, J., and Fu, D. (2009) *Nat. Struct. Mol. Biol.* **16,** 1063–1067
25. Mancia, F., and Love, J. (2010) *J. Struct. Biol.* **172,** 85–93
26. Punta, M., Love, J., Handelman, S., Hunt, J. F., Shapiro, L., Hendrickson, W. A., and Rost, B. (2009) *J. Struct. Funct. Genomics* **10,** 255–268
27. Studier, F. W. (2005) *Protein Expr. Purif.* **41,** 207–234
28. Chao, Y., and Fu, D. (2004) *J. Biol. Chem.* **279,** 12043–12050
29. Wei, Y., Li, H., and Fu, D. (2004) *J. Biol. Chem.* **279,** 39251–39259
30. Wei, Y., and Fu, D. (2005) *J. Biol. Chem.* **280,** 33716–33724
31. Wei, Y., and Fu, D. (2006) *J. Biol. Chem.* **281,** 23492–23502
32. Geertsma, E. R., Nik Mahmood, N. A., Schuurman-Wolters, G. K., and Poolman, B. (2008) *Nat. Protoc.* **3,** 256–266
33. Apell, H. J., and Bersch, B. (1987) *Biochim. Biophys. Acta* **903,** 480–494

34. Pressman, B. C., Harris, E. J., Jagger, W. S., and Johnson, J. H. (1967) *Proc. Natl. Acad. Sci. U.S.A.* **58,** 1949–1956
35. Hille, B. (2001) *Ion Channels of Excitable Membranes,* pp. 445–449, Sinauer Associates Inc., Sunderland, MA
36. Elias, C. L., Xue, X. H., Marshall, C. R., Omelchenko, A., Hryshko, L. V., and Tibbits, G. F. (2001) *Am. J. Physiol. Cell Physiol.* **281,** C993–C1000
37. Schmitt, B. M., and Koepsell, H. (2005) *J. Biol. Chem.* **280,** 24481–24490
38. Negulescu, P. A., and Machen, T. E. (1990) *Methods Enzymol.* **192,** 38–81
39. Kano, K., and Fendler, J. H. (1978) *Biochim. Biophys. Acta* **509,** 289–299
40. Finney, L. A., and O'Halloran, T. V. (2003) *Science* **300,** 931–936
41. Paulsen, I. T., and Saier, M. H., Jr. (1997) *J. Membr. Biol.* **156,** 99–103
42. Grass, G., Otto, M., Fricke, B., Haney, C. J., Rensing, C., Nies, D. H., and Munkelt, D. (2005) *Arch. Microbiol.* **183,** 9–18
43. Lu, M., and Fu, D. (2007) *Science* **317,** 1746–1748
44. Sekler, I., Sensi, S. L., Hershfinkel, M., and Silverman, W. F. (2007) *Mol. Med.* **13,** 337–343
45. Ohana, E., Hoch, E., Keasar, C., Kambe, T., Yifrach, O., Hershfinkel, M., and Sekler, I. (2009) *J. Biol. Chem.* **284,** 17677–17686